Optimal motion control for collision avoidance at Left Turn Across Path/Opposite Direction intersection scenarios using electric propulsion

To appear in *Vehicle System Dynamics*
Vol. 00, No. 00, Month 20XX, 1–28

Optimal Motion Control for Collision Avoidance at LTAP/OD Intersection Scenarios using Electric Propulsion

Adithya Arikere[ad]*, Derong Yang[b] and Matthijs Klomp[cd]

[a] *American Axle & Manufacturing, Inc,*
Trollhättan Technical Center,
Gunnar W Anderssons Passage 25,
SE-461 53 Trollhättan, Sweden
adithya.arikere@aam.com
+46 72 550 15 89

[b] *Volvo Car Corporation,*
Vehicle Motion & Control,
Gunnar Engellaus Väg PVV1:1,
SE-405 31 Gothenburg, Sweden
derong.yang@volvocars.com
+46 72 371 79 76

[c] *Volvo Car Corporation,*
Vehicle Dynamics CAE,
Gunnar Engellaus Väg PVV1:1,
SE-405 31 Gothenburg, Sweden,
matthijs.klomp@volvocars.com
+46 72 371 73 56

[d] *Chalmers University of Technology*
Mechanics and Maritime Sciences,
Hörsälsvägen 7A,
SE-412 96 Gothenburg, Sweden
<first name>.<last name>@chalmers.se

(30th Oct 2017)

Acknowledgements

The authors would like to gratefully acknowledge the contributions of Bengt Jacobson (Chalmers), Mathias Lidberg (Chalmers) and Gunnar Olsson (ÅF) towards this project and paper. We would also like to thank Volvo Cars for providing the simulation model for use in this project and also for help with setting up the scenario specification. Additionally, the support of Vector, IPG and Tomlab in providing educational licenses for the measurement, simulation and optimal control software respectively is gratefully acknowledged. Finally, we would like to acknowledge the support of our project partner American Axle and Manufacturing (AAM).

Funding

We would like to thank Vinnova of the Fordonsstrategisk Forskning och Innovation (FFI), Traffic Safety and Automated Vehicles programme for providing the funding for this project (grant no. 2015-04812).

∗Corresponding author

Collision avoidance at intersections involving a host vehicle turning left across the path of an oncoming vehicle (Left Turn Across Path/Opposite Direction or LTAP/OD) have been studied in the past, but mostly using simplified interventions and rarely considering the possibility of crossing the intersection ahead of a bullet vehicle. Such a scenario where the driver preference is to avoid a collision by crossing the intersection ahead of a bullet vehicle is considered in this work. The optimal vehicle motion for collision avoidance in this scenario is determined analytically using a particle model within an optimal control framework. The optimal manoeuvres are then verified through numerical optimisations using a two-track vehicle model, where it was seen that the wheel forces followed the analytical global force angle result independently of the other wheels. A Modified Hamiltonian Algorithm (MHA) controller for collision avoidance that uses the analytical optimal control solution is then implemented and tested in CarMaker simulations using a validated Volvo XC90 vehicle model. Simulation results showed that collision risk can be significantly reduced in this scenario using the proposed controller, and that more benefit can be expected in scenarios that require larger speed changes.

Keywords: Collision avoidance, Integrated vehicle motion control, Intersection accidents, Driver assistance systems, Optimal control, LTAP/OD

1. Introduction

Intersection accidents are one of the most common accident types in the world. In both the US and Europe, they account for approximately 40% of all accidents [1, 2]. When considering only fatal crashes, they account for approximately a fourth and a fifth of all traffic fatalities in the US [3] and Europe [4] respectively. In Sweden, while the share of intersection accidents among all accidents is relatively low at only 22.3%, they account for 17% and 21.9% of all traffic fatalities and severe injuries respectively [5][1].

While intersection accidents account for a large proportion of accidents and injuries, there are numerous sub-categories of the same with different types of intersections (T-junction, 4-way, Y-junction, etc.), signalized vs non-signalized, direction of bullet vehicle, other traffic, etc. All these factors have significant impact on the dynamics involved, threat detection and decision making. This makes analysis of intersection accidents cumbersome and time-consuming.

Fortunately, previous research on this accident scenario have highlighted a few variations that are overrepresented in the accident statistics. The two most common variants identified by [6] are called "Straight Crossing Paths" (SCP) and "Left Turn Across Path - Opposite Direction conflict" (LTAP/OD). In a NHTSA report, these accidents were ranked second and third respectively in both comprehensive societal cost and functional years lost metrics[2] [7]. In this work, in order to limit the scope, we opt to focus on the LTAP/OD crash variant. This choice is motivated by the fact that accident avoidance while cornering poses vehicle dynamic challenges that are not seen in the SCP scenario. An illustration of the LTAP/OD scenario considered in this work is shown in Figure 1.

Collision avoidance in this scenario has been studied in the past and a large body of work exists that deal with cooperative collision avoidance using vehicle-to-vehicle (V2V) or vehicle-to-infrastructure (V2I) communication [8–13]. However, one cannot always rely on all vehicles having fully functioning V2V or V2I communication systems. This is particularly true for the near future as there will likely be older vehicles on the roads that do not have such systems for some time to come [14]. The same is also true for

[1]The Swedish numbers do not include roundabouts and are for intersections only.
[2]LTAP/OD was split into non-signalised and signalised sub-categories and ranked 6 and 7 respectively in the report. When combined, they rank third in both societal cost and functional years lost.

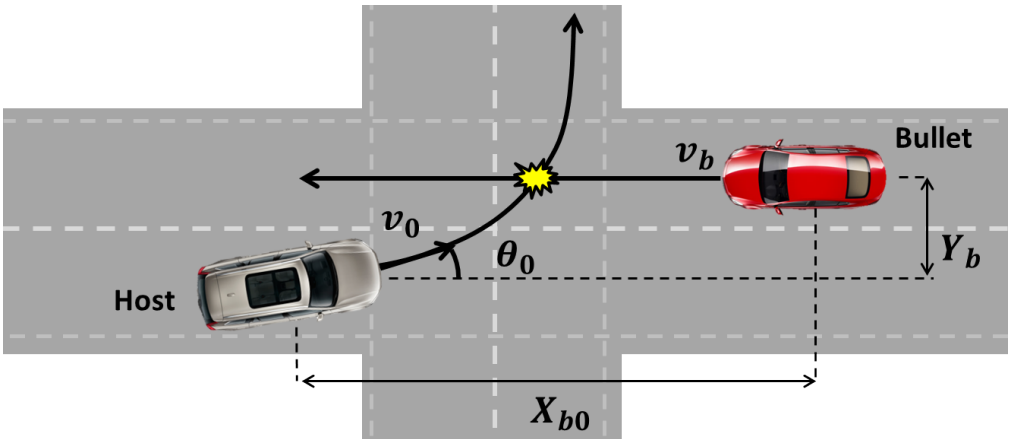

Figure 1 Schematic of the LTAP/OD intersection accident. The "opposite direction" descriptor is for the direction from which the bullet vehicle approaches the host vehicle. Here, v_0 and θ_0 are the initial velocity and course angle of the host vehicle respectively, v_b and Y_b the initial velocity and lateral offset relative to the host of the bullet vehicle respectively, and X_{b0} the initial X-distance between the host and bullet vehicles.

less common classes of vehicles such as mopeds and other non-motorised road users like cyclists and pedestrians.

Other work exists that deal with decision making for such accidents using model-based methodology, probabilistic methods, etc. [15–22]. However these use simplified motion models and/or simple manoeuvres (braking or steering only as opposed to combined braking and steering) to perform their analysis. Moreover, most of them only deal with decision making and not with vehicle control during the intervention itself. In [23], optimal control based advanced driver assistance systems (ADAS) are dealt with in general but intersection accidents are not considered specifically. They pre-compute a set of optimal manoeuvres offline and select one for use in the scenario of interest which is executed via a PID controller. In [24], Model Predictive Control (MPC) is used to perform evasive manoeuvres, however, the path planning is done outside the MPC and simplified linearised models are used in the MPC to perform path following. Moreover, brake based collision avoidance systems for intersections are already on the market [25].

To the best of the authors' knowledge, no work so far has dealt with the task of comprehensive online vehicle motion control taking into account the dynamics involved in the LTAP/OD scenario, particularly with regards to the possibility of assisting the driver if he/she decides to avoid the collision by crossing the intersection ahead of the bullet vehicle. The present work addresses this issue.

The availability of electric propulsion, either in the form of fully electric or a hybrid drivetrain, is assumed in this work. Since the manoeuvre is near-crash and is of a short duration ($\sim 1.5\,\mathrm{s}$), good controllability and fast response is needed from the propulsion actuator. Internal combustion engines are relatively less accurate to control and their response is inconsistent since it can greatly depend on factors such as gear selected, turbo lag, engine rpm, etc. Consequently, an electrified drivetrain is assumed to be able to deliver the requested torque quickly and reliably.

In this work, we formulate the problem using a particle model in an optimal control scheme to find optimal manoeuvres that avoid accidents by crossing the intersection ahead of the bullet vehicle. We assume in this work that the driver intention is to cross the intersection ahead of the bullet vehicle and as a result, solutions that override the driver (brake based solutions) are not investigated. The results so obtained are verified

through numerical optimisations[3] using the same particle model, followed by a two-track vehicle model. Results from the two-track model are analysed and compared to that of the analytical particle model. Finally, a Modified Hamiltonian Algorithm (MHA) controller is used as a torque allocation strategy that uses the analytical optimal control solution to perform driver assist interventions in this accident scenario. This controller is then tested in a high fidelity CarMaker simulation using a validated Volvo XC90 vehicle model.

2. Analytical study of the LTAP/OD scenario

While the scenario parameters vary widely in the statistics, to limit the scope of work, we focus on the scenario specified in Table 1. This specification is mainly based on an internal study performed at Volvo Cars using the Volvo Cars Accident Database but is also loosely based on on the numbers presented in [7, 26, 27]. Note that the friction level is set so as to make the manoeuvre on-limit since this introduces additional challenges for yaw stabilisation during the intervention. This scenario specification is such that, in the absence of an intervention, a conflict occurs between the rear three-quarters of the host and the front of the bullet vehicle (see Figure 12). In this case, braking might not be optimal either as a braking intervention of the wrong magnitude or executed at the wrong time can put the host vehicle firmly in the bullet vehicle's path and exacerbate the situation.

Table 1. Specification for the LTAP/OD scenario considered in this work

Parameter	**Value**
Initial host velocity (v_0)	30 km/h
Bullet vehicle velocity (v_b)	40 km/h
Initial lateral offset (Y_b)	5 m
Turn radius (R_{road})	14 m
Initial course angle (θ_0)	0°
Road surface friction (μ)	0.5
Initial X-distance between host and bullet vehicles (X_{b0})	35 m

2.1. *Manoeuvre for collision avoidance by crossing the intersection*

In this manoeuvre, the goal is to avoid the collision by crossing the intersection *ahead of* the bullet vehicle. This manoeuvre can be used as a basis for performing driver assist interventions when the driver intention is to cross, instead of to halt before the intersection. It can also be used to perform decision making in autonomous interventions or to perform the interventions themselves once the decision to pass the intersection has already been taken. Lastly, it can also be useful to perform interventions in cases when there is insufficient distance to brake to a halt before the intersection.

A schematic of this scenario as used in the optimal control formulation is shown in Figure 2. The X-distance between the host and the bullet at the end of the manoeuvre when the host vehicle crosses the global-Y position of the bullet vehicle is termed the *distance margin* and is taken as the objective function to be maximised. Note that while the road boundaries are shown in the figure, they are not considered in the problem formulation since such constraints would make it infeasible to solve the problem analytically. Potential ways to handle path constraints are discussed later in Section 2.2.

[3] A `MATLAB` based optimal control software called `PROPT` from Tomlab is used for this purpose

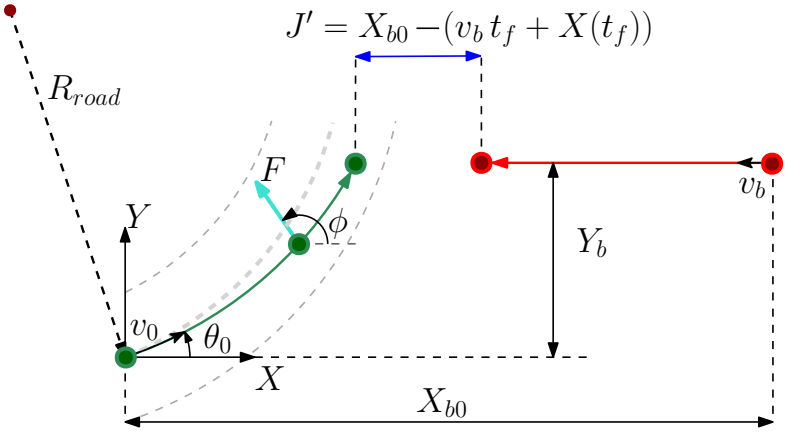

Figure 2 Distance between the two vehicles at the end of the manoeuvre is taken as the objective function. The end of the manoeuvre is defined by when the host vehicle reaches the bullet vehicle Y-position.

The optimal control problem is set up as the maximisation of the following objective function:

$$J' = X_{b0} - (v_b t_f + X(t_f)) \tag{1}$$

It is important to keep in mind that, with this formulation, an intervention will simply increase the distance margin without any consideration as to how that affects safety. Care needs to be taken in the decision making module to ensure that increasing distance margin actually improves safety. For instance, if the intervention is executed in a scenario where the bullet vehicle would have passed *ahead* of the bullet vehicle, the intervention could end up putting the host vehicle squarely in the bullet vehicle path. The decision making module should ensure that the intervention is executed only when the intervention can be expected to improve safety.

In Equation (1), since X_{b0}, the initial distance between the host and the bullet vehicle is constant, the optimal control problem can be reforumlated as a minimisation problem as follows:

$$\min_{\boldsymbol{\gamma}\in\mathcal{U}} J = (v_b t_f + X(t_f)) \tag{2a}$$

$$\text{subj. to:} \quad \boldsymbol{x}(0) = \begin{bmatrix} 0 & 0 & v_0\cos\theta_0 & v_0\sin\theta_0 \end{bmatrix}^{\mathsf{T}} \tag{2b}$$

$$p_1(\boldsymbol{x}(t_f)) = Y(t_f) - Y_b = 0 \tag{2c}$$

$$\dot{\boldsymbol{x}} = \boldsymbol{f}(\boldsymbol{x}(t), \boldsymbol{\gamma}(t), t) \quad \forall t \in [0, t_f] \tag{2d}$$

Here, $\boldsymbol{\gamma}$ is the vector of control inputs containing the total force acting on the particle and global angle of said force, that to be optimised over the time interval $t \in [0, t_f]$. $\boldsymbol{x}(0)$ is the initial condition, p_1 (or $\boldsymbol{p}$ in general for a set of constraints) is the terminal constraint and $\dot{\boldsymbol{x}} = \boldsymbol{f}$ are the dynamic constraints. Specifically, $\boldsymbol{f}$ represents the vehicle model and

can be expressed as follows:

$$\boldsymbol{f}(\boldsymbol{x},\boldsymbol{\gamma},t) = \mathbf{A}\boldsymbol{x} + \mathbf{q}(\boldsymbol{\gamma}) \quad \forall \boldsymbol{\gamma} \in \mathcal{U} \tag{3a}$$

$$\boldsymbol{x} = \begin{bmatrix} X & Y & \dot{X} & \dot{Y} \end{bmatrix}^{\mathsf{T}} \tag{3b}$$

$$\boldsymbol{\gamma} = \begin{bmatrix} F & \phi \end{bmatrix}^{\mathsf{T}} \tag{3c}$$

$$\mathbf{A} = \begin{bmatrix} \mathbf{0}_{2\times 2} & \mathbf{I}_{2\times 2} \\ \mathbf{0}_{2\times 2} & \mathbf{0}_{2\times 2} \end{bmatrix} \tag{3d}$$

$$\mathbf{q}(\boldsymbol{\gamma}) = F/m \begin{bmatrix} \mathbf{0}_{2,1} \\ \cos\phi \\ \sin\phi \end{bmatrix} \tag{3e}$$

The augmented objective function to be minimised that incorporates the constraints can then be written as ($\boldsymbol{\eta}$ and $\boldsymbol{\lambda}$ are the *Lagrange multipliers* for the terminal and system constraints respectively):

$$\begin{aligned} \hat{J} &= J + \boldsymbol{\eta}^{\mathsf{T}}\boldsymbol{p}(\boldsymbol{x}_{t_f}) + \int_0^{t_f} \boldsymbol{\lambda}^{\mathsf{T}}(\boldsymbol{f}(\boldsymbol{x}(t),\boldsymbol{\gamma}(t),t) - \dot{\boldsymbol{x}})\,\mathrm{d}t \\ &= v_b t_f + X(t_f) + \eta_1(Y(t_f) - Y_b) + \int_0^{t_f} \boldsymbol{\lambda}^{\mathsf{T}}(\mathbf{A}\boldsymbol{x} + \boldsymbol{q}(\boldsymbol{\gamma}) - \dot{\boldsymbol{x}})\,\mathrm{d}t \end{aligned} \tag{4}$$

We now introduce the Hamiltonian function as follows:

$$\begin{aligned} H(\boldsymbol{x},\boldsymbol{\gamma},\boldsymbol{\lambda},t) &= \boldsymbol{\lambda}^{\mathsf{T}}\boldsymbol{f}(\boldsymbol{x}(t),\boldsymbol{\gamma}(t),t) \\ &= \lambda_1\dot{X} + \lambda_2\dot{Y} + F/m(\lambda_3\cos\phi + \lambda_4\sin\phi) \end{aligned} \tag{5}$$

where $\boldsymbol{\lambda}$ is called the co-state of the system.

Integrating the last term $-\boldsymbol{\lambda}^{\mathsf{T}}\dot{\boldsymbol{x}}$ by parts to eliminate $\dot{\boldsymbol{x}}$ and introducing the Hamiltonian function gives:

$$\begin{aligned} \hat{J} &= v_b t_f + X(t_f) + \eta_1(Y(t_f) - Y_b) \\ &\quad - \boldsymbol{\lambda}^{\mathsf{T}}(t_f)\boldsymbol{x}(t_f) + \boldsymbol{\lambda}^{\mathsf{T}}(0)\boldsymbol{x}(0) + \int_0^{t_f} (H + \dot{\boldsymbol{\lambda}}^{\mathsf{T}}\boldsymbol{x})\,\mathrm{d}t \end{aligned} \tag{6}$$

From standard optimal control theory, the optimum can now be determined by finding the stationary point of the augmented objective function [28]. This gives the necessary conditions for the optimum (*Pontryagin's Maximum (or minimum) Principle*).

Derivative with respect to $\boldsymbol{\lambda}$ returns the system equations:

$$\begin{aligned} \frac{\partial \hat{J}}{\partial \boldsymbol{\lambda}} &= \frac{\partial H}{\partial \boldsymbol{\lambda}} - \dot{\boldsymbol{x}} = 0 \\ &= \boldsymbol{f}(\boldsymbol{x},\boldsymbol{\gamma},t) - \dot{\boldsymbol{x}} = 0 \end{aligned} \tag{7}$$

Taking the derivative with respect to the states gives the co-state dynamics:

$$\begin{aligned} \frac{\partial \hat{J}}{\partial \boldsymbol{x}} &= \frac{\partial H}{\partial \boldsymbol{x}} + \dot{\boldsymbol{\lambda}}^{\mathsf{T}} = 0 \\ \Rightarrow \dot{\boldsymbol{\lambda}} &= \begin{bmatrix} 0 & 0 & -\lambda_1 & -\lambda_2 \end{bmatrix}^{\mathsf{T}} = 0 \end{aligned} \tag{8}$$

Integrating the above equation gives:

$$\boldsymbol{\lambda} = \begin{bmatrix} C_1 & C_2 & -C_1 t + C_3 & -C_2 t + C_4 \end{bmatrix}^{\mathsf{T}} \tag{9}$$

Derivative with respect to $x(t_f)$ gives the first transversality condition:

$$\begin{aligned} \frac{\partial \hat{J}}{\partial \boldsymbol{x}(t_f)} &= \left(\frac{\partial J}{\partial \boldsymbol{x}(t_f)} + \boldsymbol{\eta}^{\mathsf{T}} \frac{\partial \boldsymbol{p}}{\partial \boldsymbol{x}(t_f)} - \boldsymbol{\lambda}^{\mathsf{T}}(t_f) \right) = 0 \\ \Rightarrow \boldsymbol{\lambda}(t_f) &= \begin{bmatrix} 1 & \eta_1 & 0 & 0 \end{bmatrix}^{\mathsf{T}} \end{aligned} \tag{10}$$

Solving for the constants in Equation (9) using Equation (10) gives:

$$C_1 = 1, \quad C_2 = \eta_1, \quad C_3 = t_f, \quad C_4 = \eta_1 t_f \tag{11}$$

$$\boldsymbol{\lambda} = \begin{bmatrix} 1 & \eta_1 & (t_f - t) & \eta_1 (t_f - t) \end{bmatrix}^{\mathsf{T}} \tag{12}$$

Differentiating with respect to t_f gives the second transversality condition:

$$\begin{aligned} \frac{\partial \hat{J}}{\partial t_f} &= \frac{\partial J}{\partial t_f} + H(t_f) + \boldsymbol{\eta}^{\mathsf{T}} \frac{\partial \boldsymbol{p}}{\partial t_f} = 0 \\ &= v_b + \dot{X}(t_f) + \eta_1 \dot{Y}(t_f) = 0 \\ \Rightarrow \eta_1 &= -\frac{v_b + \dot{X}(t_f)}{\dot{Y}(t_f)} \end{aligned} \tag{13}$$

Finally, taking the derivative with respect to the control inputs and substituting expressions for λ_3 and λ_4 from Equation (12) gives the final necessary condition:

$$\begin{aligned} \frac{\partial \hat{J}}{\partial \boldsymbol{\gamma}} &= \frac{\partial H}{\partial \boldsymbol{\gamma}} = 0 \\ &= F/m(-\lambda_3 \sin\phi + \lambda_4 \cos\phi) = 0 \\ \Rightarrow \frac{\lambda_4}{\lambda_3} &= \eta_1 = \tan\phi \end{aligned} \tag{14}$$

Note that since F appears linearly in the equation, according to Pontyagrin's maximum principle, H is minimised by setting F to its boundary value, i.e., $F = \mu m g$.

Integrating the model to get $\dot{X}$ and $\dot{Y}$ and applying the initial conditions:

$$\dot{X} = F/m \cos\phi\, t + v_0 \cos\theta_0 \tag{15}$$

$$\dot{Y} = F/m \sin\phi\, t + v_0 \sin\theta_0 \tag{16}$$

Applying the above equations to get η_1:

$$\tan\phi = -\frac{v_b + \mu g t_f \cos\phi + v_0 \cos\theta_0}{\mu g t_f \sin\phi + v_0 \sin\theta_0}$$
$$\Rightarrow \mu g t_f + v_b \cos\phi + v_0(\sin\phi\sin\theta_0 + \cos\phi\cos\theta_0) = 0 \tag{17}$$

This equation can also be used to determine t_f once ϕ is known.

Integrating the model to get Y and applying the final condition, Equation (2c):

$$\mu g \sin\phi \; t_f^2/2 + v_0 \sin\theta_0 \; t_f - Y_b = 0 \tag{18}$$

Solving Equations (17) and (18) for ϕ gives a function:

$$g(\phi) = (v_b\cos\phi + v_0\cos(\phi-\theta_0))(v_b\sin(2\phi) + v_0(\sin(2\phi-\theta_0) - 3\sin(\theta_0))) - 4\mu g Y_b = 0 \tag{19}$$

This equation may be difficult to solve analytically, but easy to solve numerically.

For the specialised case considered here where $\theta_0 = 0$, the equation reduces to:

$$\sin\phi \;\cos^2\phi\;(v_0+v_b)^2 = 2\mu g Y_b \tag{20}$$

The second derivative of the Hamiltonian needs to be checked to eliminate maximas:

$$\begin{aligned}\frac{\partial^2\hat{J}}{\partial\gamma^2} &= \frac{\partial^2 H}{\partial\gamma^2} > 0\\ &= -F/m(\lambda_3\cos\phi + \lambda_4\sin\phi) > 0\\ &= (\cos\phi + \tan\phi\sin\phi) < 0\end{aligned} \tag{21}$$

Note that this is a necessary, but not sufficient condition for a minima.

Lastly, the value of t_f from Equation (17) also needs to be checked to ensure it is positive.

Figure 3 shows the plot of Equation (19) and the optimum. It can be seen that the equation is highly non-linear with several roots. However, it can be seen that the chosen root is very close to the initial guess and can be easily obtained using a simple gradient descent search with a suitable initial guess.

Figure 4 shows the optimal paths corresponding to the solutions of Equation (19). As can be seen, even though there are multiple solutions, only one is of interest ($\phi = 112°$). The other valid root (△) is not of interest since the optimal path in this case not only leaves the road boundaries, it can also be seen that the distance margin it achieves is much less than that of the chosen root.

2.2. *Dealing with path constraints*

Since the path constraints are not explicitly considered in the optimal control problem in the previous section, it is necessary to check if the resulting optimal paths violate the path boundaries. This can be done by using the expressions for the particle path coordinates

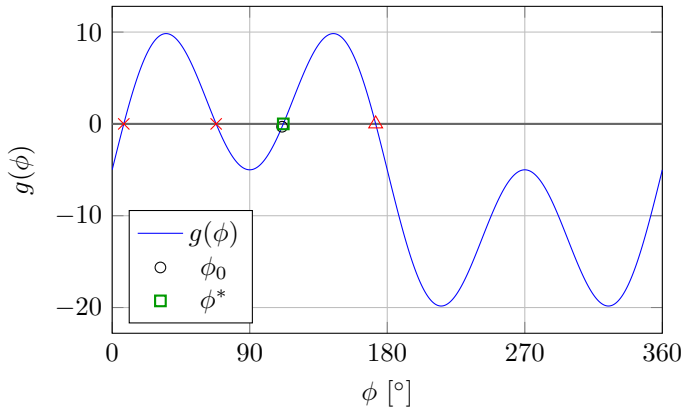

Figure 3 Plot of $g(\phi)$ (Equation (19)), the initial guess and the root corresponding to the acceleration intervention. The × marker corresponds to invalid roots (either negative final time or positive second derivative of the objective function). The △ marker corresponds to a root that is not of interest. ϕ_0 (○) and ϕ^* (□) are the initial guess and the chosen root respectively.

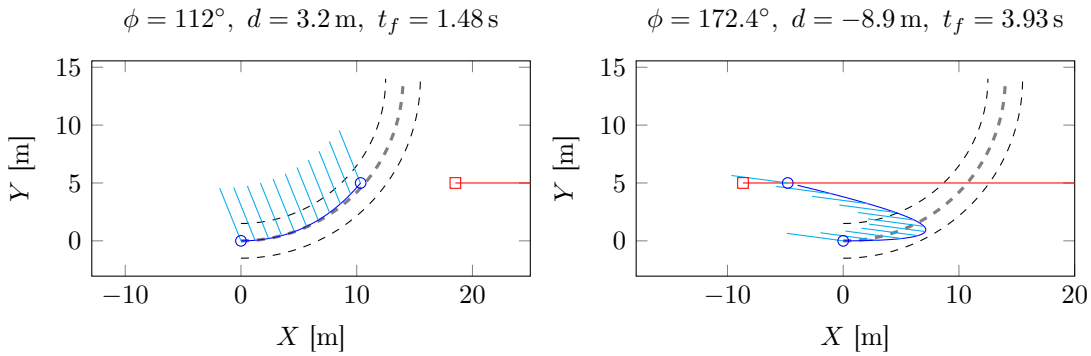

Figure 4 Optimal paths corresponding to (left) the chosen optimal root (ϕ^*, □), and (right) the other valid root (△) from the plot shown in Figure 3. Host vehicle is shown in blue, bullet vehicle in red and the vehicle global forces in cyan.

to check if the final position is outside the road boundaries.

$$X(t) = \mu g \cos\phi\ t^2/2 + v_0 \cos\theta_0\ t \tag{22}$$

$$Y(t) = \mu g \sin\phi\ t^2/2 + v_0 \sin\theta_0\ t \tag{23}$$

For a more rigours check, the path coordinates can be checked for a range of time instances $t_i \in [0, t_f]$.

Shown in Figure 5 are two examples of the final positions of the optimal paths being outside the road boundaries. The left panel shows a case of relatively slow oncoming vehicle and an excess of available grip. As a result, the grip is utilised to take a turn that is tighter than the road curvature. Conversely, the right panel shows a case of relatively fast moving oncoming vehicle and insufficient grip. Consequently, the particle offtracks and crosses the outer road edge.

Once it is seen that the final position of the particle is outside the road boundaries, the optimal control problem can be augmented with an additional constraint so as to hit the road boundary of interest at the terminal time. The optimal control problem then

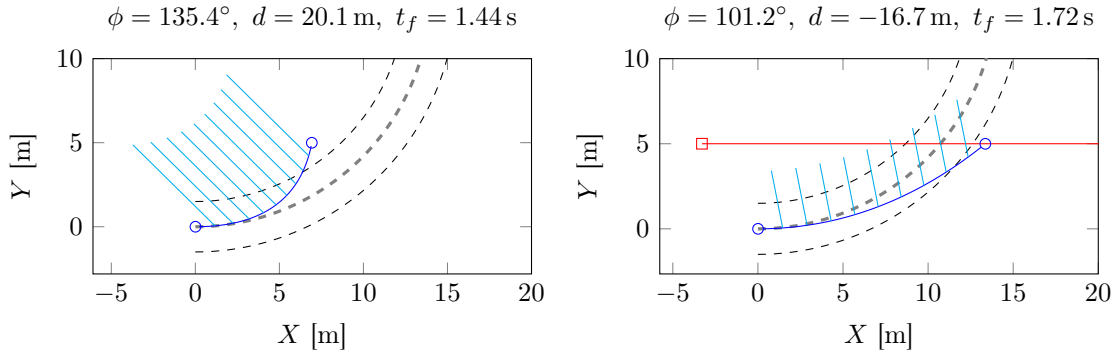

Figure 5 Optimal paths (left) for a case with $\mu = 0.7$ and $v_b = 20\,\text{km/h}$ and (right) for a case with $\mu = 0.35$ and $v_b = 80\,\text{km/h}$

becomes:

$$\min_{\boldsymbol{\gamma}\in\mathcal{U}} J = (v_b t_f + X(t_f)) \tag{24a}$$

$$\text{subj. to:} \quad \boldsymbol{x}(0) = \begin{bmatrix} 0 & 0 & v_0\cos\theta_0 & v_0\sin\theta_0 \end{bmatrix}^\mathsf{T} \tag{24b}$$

$$p_1(\boldsymbol{x}(t_f)) = Y(t_f) - Y_b = 0 \tag{24c}$$

$$p_2(\boldsymbol{x}(t_f)) = (X(t_f) - O_X)^2 + (Y(t_f) - O_Y)^2 - R_b^2 = 0 \tag{24d}$$

$$\dot{\boldsymbol{x}} = \boldsymbol{f}(\boldsymbol{x}(t), \boldsymbol{\gamma}(t), t) \quad \forall t \in [0, t_f] \tag{24e}$$

where, R_b is the radius of the road boundary of interest (inner or outer road edge) and (O_X, O_Y) are the coordinates of the center of the road segment arc.

Solving this problem in the same way as outlined in Section 2.1 gives the following expressions for the $\boldsymbol{\lambda}$ co-states and the global force angle:

$$\begin{aligned}\boldsymbol{\lambda} = \big[&1 + 2\eta_2(X(t_f) - O_X) \quad \eta_1 + 2\eta_2(Y(t_f) - O_Y)... \\ &(1 + 2\eta_2(X(t_f) - O_X))(t_f - t) \quad (\eta_1 + 2\eta_2(Y(t_f) - O_Y))(t_f - t)\big]^\mathsf{T}\end{aligned} \tag{25}$$

$$\frac{\partial H}{\partial \boldsymbol{\gamma}} = F/m(-\lambda_3 \sin\phi + \lambda_4 \cos\phi) = 0$$

$$\Rightarrow \tan\phi = \frac{\lambda_4}{\lambda_3} = \frac{\eta_1 + 2\eta_2(Y(t_f) - O_Y)}{1 + 2\eta_2(X(t_f) - O_X)} \tag{26}$$

Observing the problem closely and noting from Equation (26) that the optimal global force is once again a constant, we see that the problem is fully determined from the two terminal constraint equations.

First, the two terminal conditions can be used to determine the terminal X-coordinate.

$$\theta_f = \arccos\left(\frac{Y_b + R_b\cos\theta_0}{R_b}\right) \tag{27}$$

$$X(t_f) = R_b\sin\theta_f - R_{road}\sin\theta_0 \tag{28}$$

Here, θ_f is the angle subtended by the final position of the particle and the center of the road segment arc to the vertical. Once the coordinates of the final position are determined,

they can be used in Equations (22) and (23) and solved for ϕ and t_f. The validity of this approach was verified by comparing the result so obtained with those from numerical optimisations of the optimal control problem outlined in Equation (24). Comparing the two results showed that they were in fact identical.

Note that in the case of offtracking, it might be infeasible in some cases to stay within the outer road edge while crossing the bullet vehicle path due to overspeeding or low friction or both. The feasibility of staying within the road boundary can be checked using a similar optimal control based approach as outlined in [29]. If it is seen that staying within the road boundaries is infeasible, then either the intervention can be stopped/not started or the objective of the intervention can be changed to minimising offtracking instead. The derivation of an optimal global force angle reference to minimise offtracking is outlined in [29].

3. From particle model to two-track model

While the analytical results were seen to agree with the numerical optimisation results using a particle model, their validity when extended to more complex vehicle models still needs to be checked. In particular, the influence of yaw degree of freedom, which is not captured in the particle model, needs to be investigated. For this purpose, numerical optimisations are performed using a two-track 3 degree-of-freedom vehicle model with steady-state lateral and longitudinal load transfer and non-linear tyres. The results so obtained are then analysed and also compared with the particle model results.

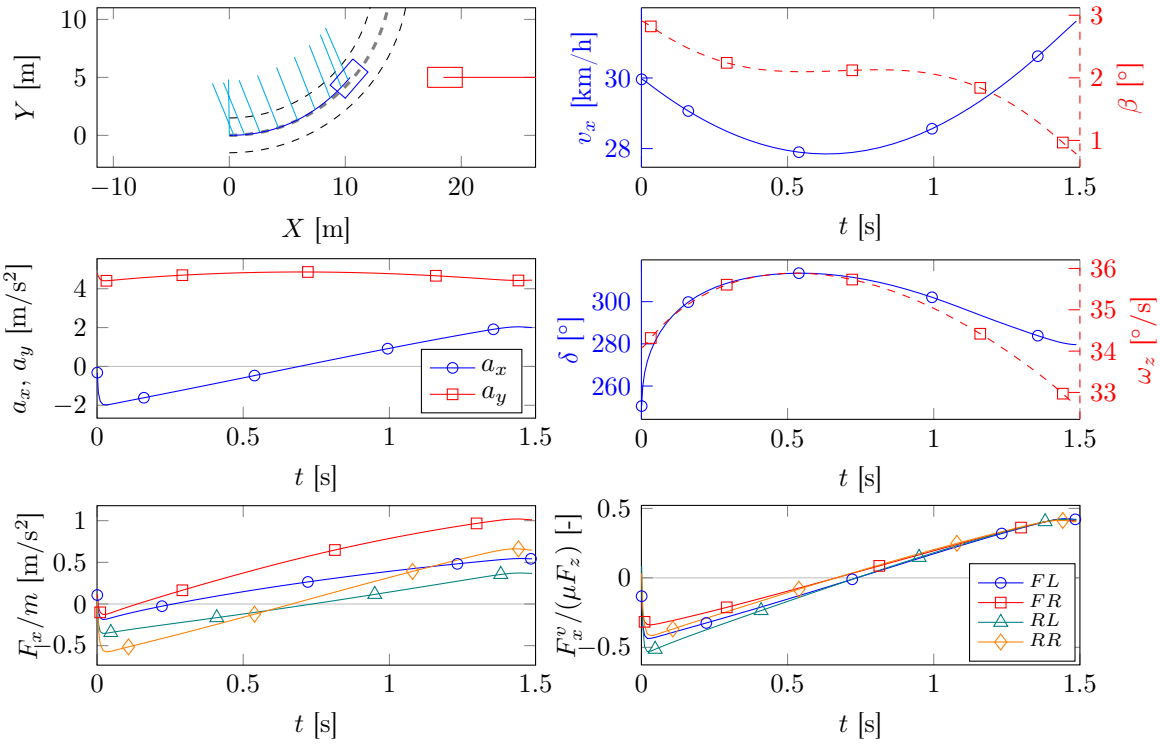

Figure 6 Results from the numerical optimisations of the two track model (no tyre force restrictions). In the bottom row, left panel shows tyre longitudinal forces in tyre reference frame normalised by vehicle mass whereas the right panel shows tyre longitudinal forces in vehicle reference frame normalised by available grip at tyre.

Figure 6 shows the results from the numerical optimisation of the two track model

when the tyre forces are unrestricted. As can be seen, the vehicle trajectory and the force vectors are very similar to that seen in the case of the particle model. The effect of the fixed obtuse global force angle as the vehicle goes through the manoeuvre can be seen in both the acceleration and the velocity plots. Due to the force angle initially being obtuse relative to the vehicle, it is braked during the first part of the manoeuvre. As the vehicle yaw angle changes however, the force angle becomes acute relative to the vehicle and as a result the vehicle accelerates during the latter part of the manoeuvre. From the speed plot, it can be seen that the net longitudinal speed change over the course of the manoeuvre is less than 2 km/h. A sideslip angle constraint of 6° is used in the optimisation, which as can be seen, is never active in this case.

From the longitudinal force plots, it can be seen that while they generally show the same trend as the longitudinal acceleration, they differ significantly from each other. This is partly explained by the fact that the normal loads on the tyres are different due to load transfer and partly by the need to generate a yaw moment in order to keep the vehicle turning. This can also be confirmed by looking at the plots of normalised longitudinal force in vehicle reference frame (bottom right), wherein it can be seen that they are nearly identical. The larger difference in the beginning of the normalised plots can be explained by the fact that the yaw moment requirement is greater in the beginning as the vehicle transitions from steady-state cornering (initial condition) to the optimal avoidance manoeuvre.

From the steering angle and yaw rate plots, it can be seen that they match each other very closely. This also implies that the yaw moment contribution from the wheel forces are relatively small. The shape of the steering and yaw rate plots can be explained by the longitudinal speed and lateral acceleration plots and keeping in mind the relationship between them ($a_y \approx v_x \omega_z$).

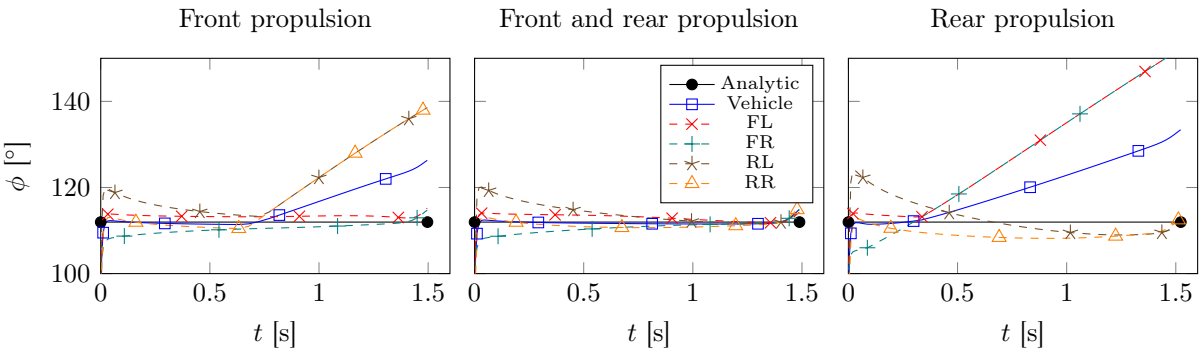

Figure 7 Global force angle of the wheels with propulsion capability restrictions

Figure 7 shows the global force angle plots for the wheels and the vehicle for different cases where propulsion is restricted to different extents. The left, centre and right panels show cases where propulsion is allowed on the front axle only, on both axles and rear axle only, respectively.

It can be seen that when there are no constraints on tyre forces that can be applied, the vehicle and the wheel global force angles track the analytical closely with less than 5° of deviation. The larger deviation initially is due to the fact that the optimisation is started with an initial condition corresponding to a steady state cornering situation and it takes a while for the vehicle forces and states to settle to the optimal solution. The deviation at the end is due to an artificial energy term that has been used in the objective function to help the program converge quickly. The small amount of deviation also indicates that the

influence of yaw moment (which is not captured in the particle model) is rather small.

The plots of the restricted propulsion cases show that the wheels track the optimum global force angle irrespective of the other wheel's performance. It can be seen that the wheels do not "collaborate" to achieve a vehicle global force angle close to the optimum. This indicates that it might be sufficient to control the tyre force angle at each wheel independently.

The results from the two-track optimisations, particularly the case of propulsion front and rear, confirm the validity of the particle model result since the deviation in global force angles of the tyres is small. Specifically, it indicates that the impact of yaw moment dynamics is small. Additionally, the cases of propulsion front or rear only, indicate that the tyre forces may be controlled independently since it is seen that the tyres independently follow the analytical force angle result irrespective of the other tyres' performance.

4. Modified Hamiltonian Algorithm (MHA) Controller for Collision Avoidance

The Modified Hamiltonian Algorithm (MHA) Controller was first formulated and presented in [30, 31] and was in turn inspired by the work in [32]. The controller is motivated by optimal control theory wherein the minimization of the objective function can be reduced to a minimization of the Hamiltonian. The MHA is used here for the purpose of wheel force allocation given the global force angle target from the analytical solution.

The choice of MHA here is motivated by the fact that it is well suited for control when virtual control target is in the form of a force angle. Further, since the MHA is based on optimal control theory, it is a natural choice as a controller since the reference is also generated using an optimal control framework. Lastly, while combined longitudinal and lateral control is typically not preferred for safety critical applications, the MHA is particularly good at it and has been shown to work well at limit handling conditions in real-world experiments [33] since it takes the detailed non-linear tyre characteristics into account.

4.1. *MHA control design*

Consider a three degree-of-freedom vehicle model in the global reference frame as follows:

$$\dot{\boldsymbol{x}} = \mathbf{A}\boldsymbol{x} + \mathbf{B}\boldsymbol{u} \tag{29}$$

$$\mathbf{A} = \begin{bmatrix} \mathbf{0}_{3\times3} & \mathbf{I}_{3\times3} \\ \mathbf{0}_{3\times3} & \mathbf{0}_{3\times3} \end{bmatrix} \quad \mathbf{B} = \begin{bmatrix} \mathbf{0}_{3\times3} \\ \mathbf{I}_{3\times3} \end{bmatrix} \tag{30}$$

$$\boldsymbol{x} = \begin{bmatrix} X & Y & \psi & \dot{X} & \dot{Y} & \dot{\psi} \end{bmatrix}^{\mathsf{T}} \tag{31}$$

$$\boldsymbol{u} = \begin{bmatrix} F_{XG}/m & F_{YG}/m & M_{ZG}/I_{zz} \end{bmatrix}^{\mathsf{T}} \tag{32}$$

where, F_{XG}, F_{YG} and M_{ZG} are the vehicle level global vehicle forces. For this vehicle model and the given problem which has a terminal time cost function, the Hamiltonian can be written as:

$$H = \boldsymbol{\lambda}^{\mathsf{T}}(\mathbf{A}\boldsymbol{x} + \mathbf{B}\boldsymbol{u}) \tag{33}$$

According to *Pontryagin's Maximum (or minimum) Principle* [28], the minimisation

of the objective function requires the minimisation of the *Hamiltonian*. Clearly, only the second term of the Hamiltonian is influenced by $\boldsymbol{u}$. Consequently, the Hamiltonian minimisation can be reduced to a minimisation of:

$$H_1 = \boldsymbol{\lambda}^{\mathsf{T}}\mathbf{B}\boldsymbol{u} \tag{34}$$

$$= \lambda_4 F_{XG}/m + \lambda_5 F_{YG}/m + \lambda_6 M_{ZG}/I_{zz} \tag{35}$$

Since F_{XG}, F_{YG} and M_{ZG} are bounded, the absolute value of the co-states do not matter for the minimisation but only their ratios. Furthermore, the ratio of the co-states corresponding to the longitudinal and lateral force has already been determined in the particle model analysis to be the tangent of the targeted global force angle (Equation (14)). Hence the Hamiltonian can be rewritten as:

$$H_1 = -\cos\phi F_{XG}/m - \sin\phi F_{YG}/m + \lambda M_{ZG}/I_{zz} \tag{36}$$

Here, λ is the co-state corresponding to the yaw moment M_{ZG} and is related to λ_6, but has been scaled to the new co-states of F_{XG} and F_{YG}. Note that we take the negative of the co-states since the goal is to maximise the vehicle global force in their direction but the problem formulation here is to minimise the Hamiltonian. The Hamiltonian can be rewritten in terms of the individual tyre force as (H_1 is renamed as H for brevity):

$$H = \sum_i -\cos\phi_v F^v_{x,i}/m - \sin\phi_v F^v_{y,i}/m + \lambda(y_i F^v_{x,i} + x_i F^v_{y,i})/I_{zz} \tag{37}$$

$$= \sum_i \left(\frac{-\cos\phi_v}{m} + \frac{\lambda y_i}{I_{zz}}\right) F^v_{x,i} + \left(\frac{-\sin\phi_v}{m} + \frac{\lambda x_i}{I_{zz}}\right) F^v_{y,i} \tag{38}$$

$$= \sum_i \cos\phi_{w,i} F^v_{x,i} + \sin\phi_{w,i} F^v_{y,i} \tag{39}$$

Here, $F^v_{x,i}$ and $F^v_{y,i}$ are the tyre forces in the vehicle reference frame and ϕ_v is the vehicle global force angle relative to the vehicle and $\phi_{w,i}$ is the wheel-corner force angle in the vehicle reference frame. Since it is convenient to work in the wheel reference frame, we transform the tyre forces from the vehicle reference frame to the wheel reference frame using the rotation matrix $\boldsymbol{R}(\delta_i)$:

$$H = \sum_i \cos\phi_{t,i} F^t_{x,i} + \sin\phi_{t,i} F^t_{y,i} \tag{40}$$

where $\phi_{t,i}$ is the force angle in the tyre reference frame and $F^t_{x,i}$ and $F^t_{y,i}$ are the tyre forces in the tyre reference frame.

The Hamiltonian can now be decomposed into individual wheel Hamiltonians that can be minimised independently assuming that the individual wheel Hamiltonians are insensitive to the applied braking forces at other wheels. Note that while there is the influence of load transfer, the wheel normal loads are estimated independently using the vehicle accelerations and are supplied to the Hamiltonian function as inputs. Additionally, the dynamics of the vehicle and suspension affects tends to damp out rapid changes in wheel normal loads.

$$H_i = \cos\phi_{t,i} F^t_{x,i} + \sin\phi_{t,i} F^t_{y,i} \tag{41}$$

In the above equation, $F^t_{x,i}$ are the optimised variables, whereas $F^t_{y,i}$ are determined using a tyre model with the wheel slip angles and $F^t_{x,i}$ as inputs. The idea that the Hamiltonians can be minimised independently at the wheel level is also supported by the numerical results from the two-track model which show that wheels and axles seem to independently follow the analytical global force angle.

To determine $\phi_{w,i}$ however, the co-state corresponding to yaw moment (λ) still needs to be determined. This can be done in an adaptive way so as to maintain the yaw balance of the vehicle through the manoeuvre. And as long as the vehicle is yaw stable, the yaw moment can be adapted to improve the performance in the scenario. First we calculate numerically the gradient of the individual tyre Hamiltonians with respect to the corresponding tyre slip angle, α_i:

$$\frac{\partial H_i}{\partial \alpha_i} = \frac{H_i(\alpha_i + \varepsilon) - H_i(\alpha_i - \varepsilon)}{2\varepsilon} \tag{42}$$

Then, using the slip equation, the gradient of the Hamiltonian with respect to the side slip angle can be determined.

$$\alpha_i \approx \delta_i - \beta - \frac{\omega_z x_i}{v_x} \tag{43}$$

$$H_\beta = \frac{\partial H}{\partial \beta} = \sum_i \frac{\partial H_i}{\partial \alpha_i}\frac{\partial \alpha_i}{\partial \beta} = -\sum_i \frac{\partial H_i}{\partial \alpha_i} \tag{44}$$

The desired side slip angle rate can then be written as:

$$\dot{\beta}^d = \begin{cases} -k_\beta \ \mathrm{sign}(\beta) & |\beta| > \beta_2 \\ 0 & |\beta| > \beta_1 \cap \beta H_\beta < 0 \\ -k_\beta \tanh(H_\beta / H_{\beta,tol}) & \text{otherwise} \end{cases} \tag{45}$$

where β_1 and β_2 are side slip angle thresholds such that $\beta_2 > \beta_1 > 0$. Next, the desired yaw rate can be written using the desired side slip angle rate and the road curvature.

$$\omega_z^d = \dot{\nu}^d - \dot{\beta}^d \tag{46}$$

$$mv\dot{\nu}^d = (F_{YG}\cos\nu + F_{XG}\sin\nu) \tag{47}$$

Finally, the desired yaw moment can be written as follows:

$$M_z^d = I_{zz}\frac{\omega_z^d - \omega_z}{\tau} \tag{48}$$

The value of λ can then be adapted as follows in order to track the desired yaw moment:

$$\lambda \to \lambda + S\tanh\Big(\epsilon \cdot (M_z - M_z^d)\Big) \tag{49}$$

In this way, the yaw moment M_z is controlled not only to maintain yaw stability but also to help minimise the objective function over the course of the manoeuvre.

For autonomous interventions, a similar method as for β can be used to determine a

desired steering wheel angle rate:

$$H_\delta = \frac{\partial H}{\partial \delta} = \frac{\partial H_1}{\partial \alpha_1}\frac{\partial \alpha_1}{\partial \delta} + \frac{\partial H_2}{\partial \alpha_2}\frac{\partial \alpha_2}{\partial \delta} = \frac{\partial H_1}{\partial \alpha_1} + \frac{\partial H_2}{\partial \alpha_2} \tag{50}$$

$$\dot{\delta}^d = -k_{\dot{\delta}} \tanh(H_\delta / H_{\delta,tol}) \tag{51}$$

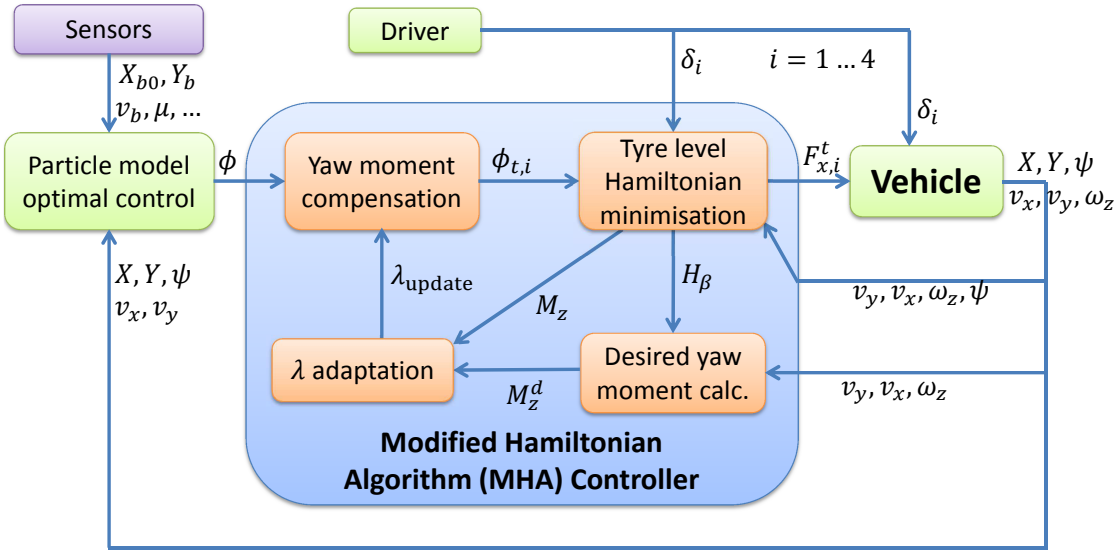

Figure 8 Structure of the Modified Hamiltonian Algorithm (MHA) controller

Figure 8 shows the overall structure of the Modified Hamiltonian Algorithm (MHA) controller. The particle model is first used to solve the analytical optimal control problem using the current vehicle states and position. The resulting global force vector direction is then transformed to the vehicle coordinates, adjusted to generate a yaw moment as necessary and then transformed to tyre coordinates. The resulting tyre force vector direction is used to minimise the Hamiltonian locally at each wheel. The resulting forces and the Hamiltonian gradient is used to calculate the current estimated and the desired yaw moment for the next iteration. These moment estimates are then used to adapt the yaw moment co-state (λ) in order to adjust the yaw moment for the next iteration.

Figure 9(a) shows the tyre models used by CarMaker and the matched tyre model used in the MHA controller. The matched model is a Magic Formula tyre model based on [34], but has been simplified for faster computation. The tyres used in CarMaker is also a Magic Formula tyre model and hence a near perfect match is possible in this case. Figure 9(b) shows the tyre force curves and the computed optima for a single iteration of the MHA. Since the tyre model used here is not isotropic, the final optimised tyre force does not have the same angle as the targeted tyre force angle. Note that the goal of the Hamiltonian minimisation is not to minimise the error in the tyre force angle, but instead to maximise the projection of the tyre force in the desired direction.

4.2. *Simulation results*

The controller outlined in the previous section was implemented in a CarMaker simulation environment with a validated Volvo XC90 vehicle model. A driver assist intervention is considered in this case. The steering performed by CarMaker's own driver model and the

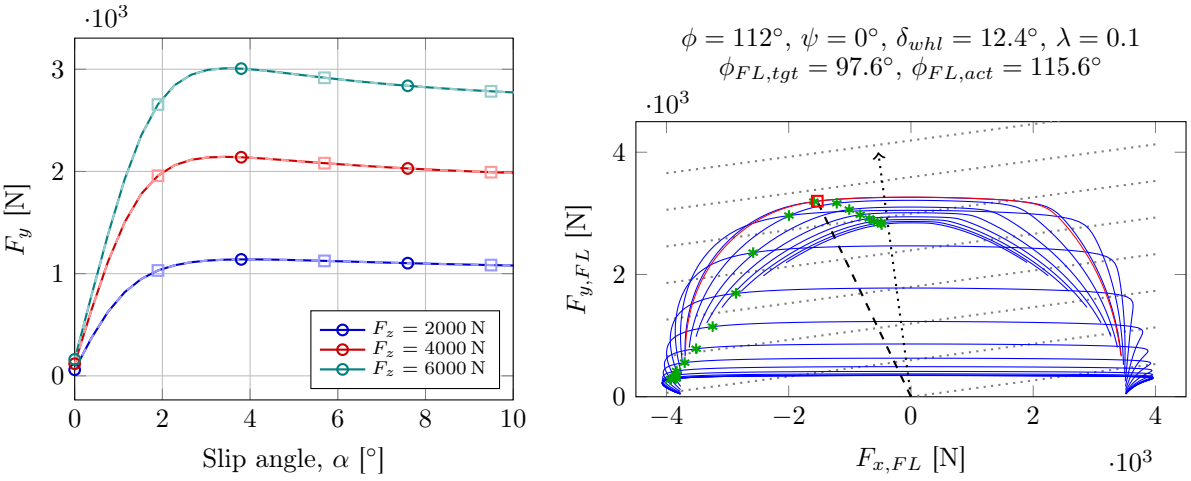

(a) Matched tyre model for $\mu = 0.5$

(b) Single iteration of MHA

Figure 9 (a) Plots of the CarMaker tyre model (—o—) and the matched tyre model (- ⊡ -) used in the MHA controller. (b) One iteration of the MHA at the left front wheel with a global force target of 112°. Grey dotted lines show contours of constant *Hamiltonian*. Green markers indicate optima along corresponding tyre force curve. Red line corresponds to tyre force curve for current slip angle. At the top, steer angle at the wheel, the targeted tyre force angle taking yaw moment considerations into account, and the actual tyre force angle achieved are shown. The dashed black line shows the angle of the optimised tyre force and the dotted black line shows the targeted force direction.

intervention is started at the beginning of the turn, i.e., at $\theta_0 = 0$. Propulsion capability is assumed on both axles as is the ability to apply individual wheel brake torques. The availability of electric propulsion and individual wheel brakes means that they can then be combined to perform torque vectoring by braking. Hence effectively, independent wheel force control capability is assumed.

The results so obtained from the simulations are compared with a case where the intersection is navigated without the controller but at constant speed. As previously mentioned, we assume in this case that the driver intention is to avoid the collision by crossing the intersection ahead of the bullet vehicle.

Figure 10 shows the simulation results from CarMaker simulations using the proposed controller and the validated XC90 vehicle model. As can be seen, the vehicle manages to avoid the bullet vehicle with a small margin. The scenario is specified such that at constant speed the bullet vehicle strikes the host vehicle in the intersection. In the tyre force plots, the dashed lines represent the request from the MHA whereas the solid lines represent the actual forces at the wheels. The tyre and the actuator dynamics cause large oscillations in the wheel fores initially. Some discrepancy is seen even at the end due to the inaccuracy in tyre radius used when converting the force requests from the MHA to torque requests for the brakes or the propulsion. Note that the actual tyre radius of each wheel changes through the manoeuvre due to load transfer.

Large variation and oscillations can also be seen in the force angles particularly in the beginning. These are partly explained by the tyre force oscillations but are also explained by the fact that the dynamics of the vehicle as a whole take some time to settle to the optimum. The tyre force oscillations are caused largely due to tyre relaxation effects and also due to the wheel dynamics. It can be seen that the force angles approach the optimum towards the end. Additionally, due to the non-isotropic nature of the tyre model, there will always be a difference between the achieved force angles and the optimum. This effect can also be seen in Figure 11 which shows the different force angles at each wheel.

As can be seen from Figure 11, several factors contribute to the force angles deviating

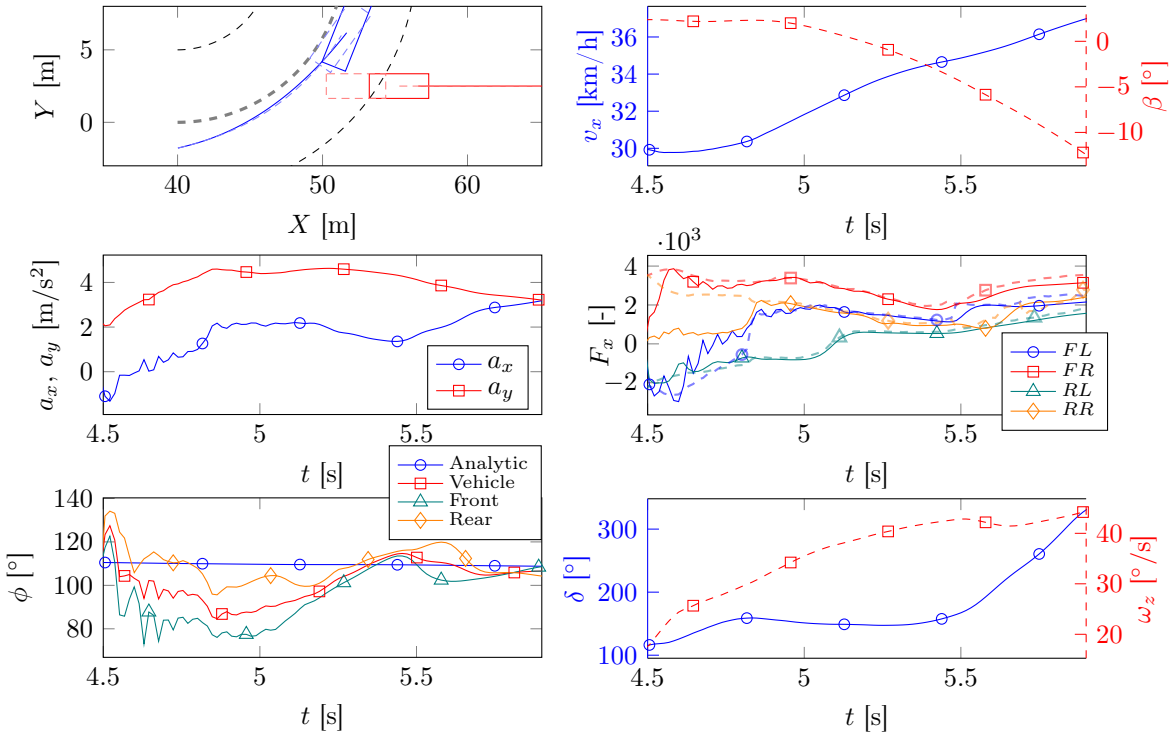

Figure 10 Simulation results with MHA controller in CarMaker and the Volvo XC90 vehicle model. In the path plot, the passive vehicle path and final positions are shown in lighter, dashed plots. In the longitudinal force plots, the dashed lighter plots represent the request from the controller and the darker ones represent the actual forces at the tyres. In the force angle plots (bottom left), the four plots refer to the analytical particle model result, full vehicle, front axle and rear axle force angles respectively from the simulation.

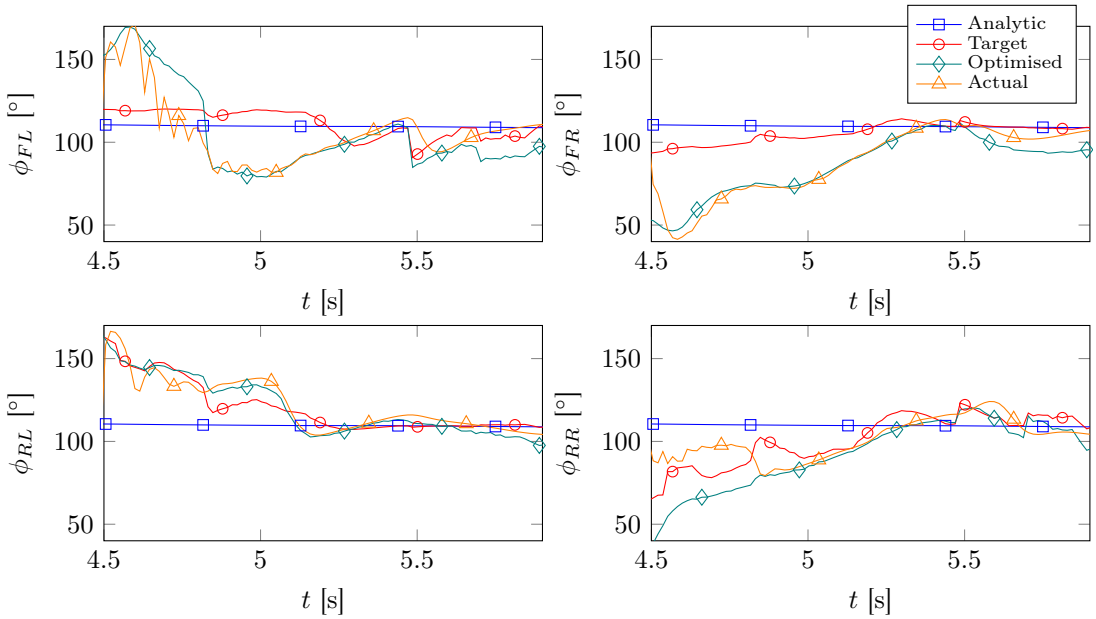

Figure 11 Global force angles at the wheels. Shown are the analytically computed angle for the whole vehicle, the wheel force angle taking yaw moment into consideration (Target), the optimised angle considering the tyre model (Optimised) and the actual angle measured from the tyre forces.

from the optimal. Depending on the wheel, the yaw moment contribution can either be near zero (front left wheel) or large (rear left) which can be interpreted from the deviation of the "target" tyre force angle plots from the "analytic". Here, the "target" curve represents the wheel force angle calculated by the MHA taking yaw moment into account whereas "analytic" refers to the analytical particle model result. This deviation is particularly dominant in the beginning of the manoeuvre. This is understandable since the yaw moment is controlled by λ-adaptation and it takes a while for this to converge. However, the biggest contributor to the deviation appears to be the tyre model itself. This can be interpreted by observing the deviation between "target" and "optimised" which is the angle calculated by the MHA taking the active tyre force curve into account. Due to the non-isotropic nature and the differences in the actual tyre model as compared to the one used in the analytical formulation, a large deviation in the force angle is observed. Another factor here is that at low slip angles (particularly at the beginning of the manoeuvre), the tyre curve is highly non-isotropic and nearly rectangular. Lastly, the dynamics of the wheels, tyres and the actuators themselves causes deviations which are observed as oscillations in the force angles. Inaccuracies in estimated tyre radius, vertical forces, etc. cause a deviation even during steady state. However as stated, it is interesting to note that the force angles follow an understandable trend, and converge to the analytical solution eventually towards the end of manoeuvre.

Figure 12 Screenshot of the host vehicle avoiding the bullet vehicle. The shaded host vehicle is the passive vehicle without an intervention.

Figure 12 shows a screenshot of the critical time instant in the scenario when the host vehicle just avoids the bullet vehicle. The shaded vehicle here represents the vehicle without the controller that performs the manoeuvre while maintaining the vehicle speed. It can be seen that maintaining speed in this scenario causes the host vehicle to be hit in the rear of the vehicle. Braking in this case is risky since it could put the vehicle squarely in the path of the bullet vehicle. It was observed that the MHA controller improved the distance margin by 1.6 m over the passive vehicle.

While path constraints (such as lane boundaries) are accounted for at the particle model level (see Section 2.2), due to differences in the actual vehicle compared to the particle model, the tyre map used, etc., deviations can arise in the actual vehicle path and as a result, path constraints may be violated by the vehicle. Depending on the type of path constraint under consideration, different options exist to ensure path constraints

are satisfied. If the vehicle is at risk of violating the outer road boundary, the method presented in [29] can be used to minimise off-tracking. On the other hand, if the vehicle is close to violating the inner road boundary, a constraint can be added in the MHA optimisation that limits the maximum lateral force that can be generated by the tyres. A more general way of dealing with path constraints can be to gradually adjust the global force angle reference by adding a vector component normal to the constraint surface. This would result in the global force angle target pointing away from the constraint and hence cause the vehicle to move away from the constraint as well. An adaptive approach such as the one used in Equation (49) for stability control can be used here.

Figure 13 shows the distance margins achieved in different cases. The left panel shows the distance margins measured between the centre of gravities of the host and bullet vehicle when the host centre of gravity is in line with the bullet vehicle path. This distance margin is the variant that is used as the objective function in the optimisation. The right panel shows the distance margin measured between the nearest points of the two vehicles when the host vehicle has fully cleared the bullet vehicle path (rear right corner of host vehicle above front right corner of bullet vehicle). While the latter is a more accurate measure of collision risk, this is not used as the objective function since adding yaw or course angle of the vehicle to the objective function results in a formulation that is infeasible to solve analytically. For the particle model, this distance margin is calculated by using a rectangle of the vehicle size attached to the particle position and course angle.

The particle model and the two-track model refer to the optimal control results where the benefit improvement is seen to be small. In this context, "Without control" means that no tyre longitudinal forces are allowed. However, it is worth noting that the manoeuvre specification is on-limit. The initial conditions are such that, initially, the vehicle is slightly overspeeding entering the corner ($v_0^2/R_{road}/(\mu g) = 1.01$). As a result, the benefit obtained is purely by better utilisation of the tyre grip and not by increased tyre grip utilisation. It is also worth noting that the "without control" cases here are still optimal, but just has more restrictive constraints on the control inputs.

In contrast, in case of the CarMaker simulations, the case of "without control" is not optimal. Furthermore, the driver model here performs corner cutting and thereby reduces the tyre grip utilisation. This allows the MHA controller to not only better utilise the tyre grip but also to increase the tyre grip utilisation and this in turn results in the larger distance margin improvement that is seen.

From the two subplots, it can be observed that the distance margin improvement is larger when measured between the nearest points. This is due to the fact that a larger distance and duration is required in order to fully clear the bullet vehicle path. This in turn allows the controller a longer duration for it to operate and maximise the distance margin.

Lastly, it is worth keeping in mind that, in this scenario, the optimal manoeuvre has a net speed change of just 2 km/h over the duration of the intervention which is approximately 1.5 s. As a result, simply maintaining speed in this scenario is not very far away from optimal. Higher distance margin improvements can be expected in scenarios that require larger speed changes over a longer intervention duration.

5. Discussion

In this section applications of the method presented in this work in other scenarios, impact of the assumptions made and limitations of this work are discussed.

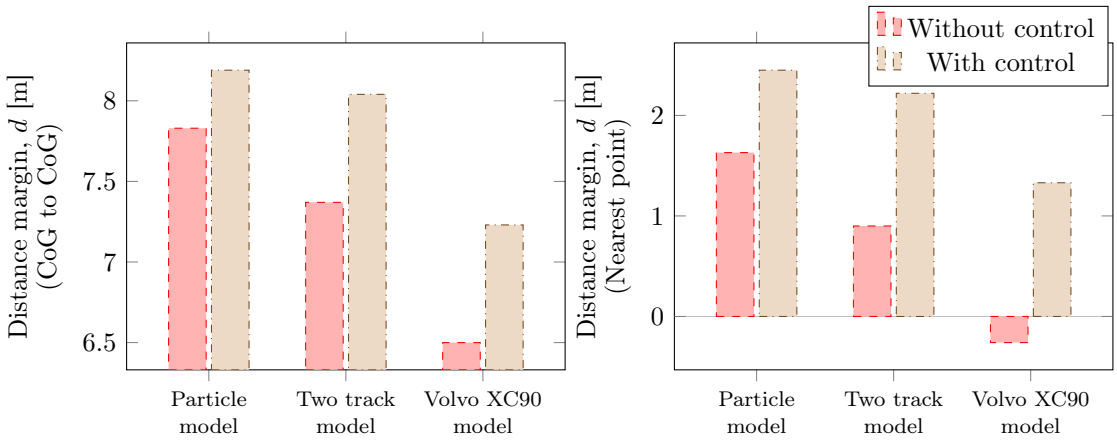

Figure 13 Left panel shows distance margins measured between the host and bullet vehicles' respective centre of gravities at the moment the host centre of gravity is in line with the bullet vehicle path. Right panel shows distance margins measured between the nearest corners of the vehicles when the rear right corner of the host vehicle is in line with the bullet vehicle front right corner.

5.1. *Applications of method for other scenarios*

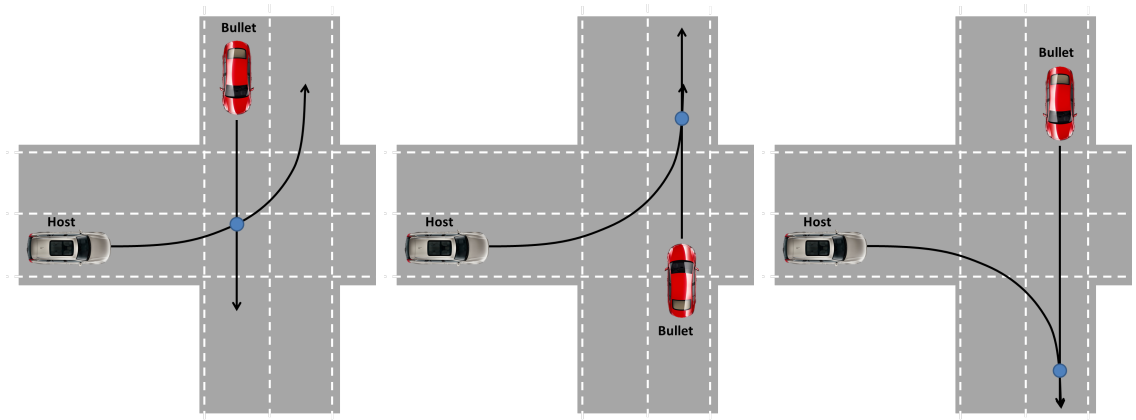

(a) Left Turn Across Path/Lateral Direction (LTAP/LD)

(b) Left Turn Into Path (LTIP)

(c) Right Turn Into Path (RTIP)

Figure 14 Intersection accidents

The methodology described in this work can also be used in other intersection accidents such as those shown in Figure 14 where yaw moment control and longitudinal control need to be performed simultaneously. The objective function and the initial and final conditions will need to be adapted in each case to reflect the scenario, but the rest of the method outlined in this work can be applied.

5.2. *Actuator limitations*

While actuator limitations are not considered in this work, their impact on the results are expected to be minor. Since both the brakes and electric drives are fast actuators, not considering their rate limits is likely to have had little impact. Furthermore, as seen in the force requests plots in Figure 10, the requests don't change rapidly. The electric drive torque too are unlikely to had much impact for several reasons. First, the max acceleration

achieved in this intervention is only $2\,\mathrm{m/s^2}$ (see Figure 10). Second, the intervention is performed at relatively low speeds (max $37\,\mathrm{km/h}$) and since electric drives deliver their peak torques at low speeds, their peak torque limitations are unlikely to be limiting in this case.

If needed however, the MHA controller can easily take magnitude limitations of wheel actuators into account. This is done by simply restricting the search in the Hamiltonian to the longitudinal force domain of interest.

For magnitude limitations caused by open differentials or other differentials, the minimisation needs to be performed for the axle as a whole. This can be done in two stages: first find the optimum longitudinal force for each wheel as usual, then search the space defined by the two individual wheel optimum longitudinal forces to find a common longitudinal force for the two wheels that minimises the axle Hamiltonian. Since the axle Hamiltonian is still only a linear sum of the wheel Hamiltonians, this adds just one more linear search to the controller.

The MHA is unable to directly take actuator rate limitations into account. However, as in the case of the steering angle, the derivative of the Hamiltonian with respect to the actuator input of interest can be used to control the rate of actuation of such inputs.

5.3. *Electric drive benefit*

Clearly, as shown in the results, accurate and fast actuation capability is needed not only to be able to accurately control the force angle, but also since the manoeuvre itself is only $1.5\,\mathrm{s}$ long in this case, fast actuators are needed to deliver the requested torques in time. An internal combustion (IC) engine is less suitable here since they not only have slow response but are have inconsistent response due to possibly being in the wrong engine rpm range, turbo lag, automatic gearbox, etc. An electric drive on the other hand is well suited here.

Furthermore, the availability of such a fast propulsion actuator allows it to be combined with individual wheel braking to achieve brake based torque vectoring. This can in turn be used for better yaw moment control since torque vectoring can achieve higher yaw moment magnitudes than brakes alone. On top of this, the combination of electric drive and brakes allows yaw moments to be applied without applying a net longitudinal force on the vehicle. This allows yaw moment control to be decoupled from longitudinal control leading to simpler controllers and better performance. Hence even when propulsion or acceleration is not required in an intervention, electric drives can improve the effectiveness of the intervention

5.4. *Sensor and data requirements*

In comparison to traditional vehicle control strategies, the MHA needs much more information. The major piece of information that the MHA needs that is traditionally not needed by other controllers is the tyre model. However, this is a one-time requirement and needs to be fed into the controller when it is designed. This raises several questions regarding ensuring the tyre model accuracy over time. It might be possible to continuously adapt parameters in the tyre model as the tyre behaviour changes over time due to wear, temperature, etc. Some work has been done previously on identifying tyre properties online [35]. The other question that this raises is the issue of tyre changes. In such cases, either the tyre model needs to be updated along with the tyre change or perhaps the MHA can revert to a "fallback" tyre model when it detects that the online tyre model

does not match the actual tyre behaviour.

The other major pieces of information needed are the vehicle side slip angle or velocity and the road friction level. While not covered in this work, these can be estimated online from the measurable vehicle states [36]. Particularly, the friction estimation is made easier due to the fact that the manoeuvre is an on-limit manoeuvre and hence friction can be estimated as soon as the limit is reached.

Finally, information such as the vehicle position, road boundaries, position and velocity of the bullet vehicle, etc. are needed. However the need of such information is unavoidable for such collision avoidance functions. These needs can be met through various sensors such as radar, lidar, camera vision systems or even V2V or V2I communication.

6. Conclusions

The task of vehicle motion control for collision avoidance by passing the intersection ahead of the bullet vehicle in a Left Turn Across Path/Opposite Direction (LTAP/OD) scenario is considered in this work.

The scenario is first analysed using an analytical optimal control framework using a particle model. The results so obtained regarding optimal global force angles for collision avoidance are then verified in numerical optimisations using a two-track vehicle model. The global force angle results are analysed further for different drivetrain configurations and it was found that not only does the particle result represent a good approximation of the vehicle motion in the unconstrained case, even when the tyre forces are constrained, the unconstrained tyres still attempt to follow the particle global force angle.

A vehicle dynamics controller called the Modified Hamiltonian Algorithm (MHA) controller inspired by optimal control theory and using the analytical optimal control result previously obtained is outlined. While the MHA has been used for other applications like lane changes and for mitigating understeer, its use for collision avoidance in intersection accidents represents a novel application of the algorithm. The controller is then implemented in simulation and tested in high-fidelity CarMaker simulations using a validated Volvo XC90 vehicle model. Simulations of the scenario with an driver assist intervention performed using the proposed controller showed a distance margin improvement of 1.6 m over the passive vehicle. Higher distance margin improvements can be expected in scenarios that require a larger speed change over the course of the manoeuvre. Higher improvement can also be expected when the steering is allowed to be actively controlled as well.

Lastly, while previous work has dealt with collision avoidance at intersections, they mostly used simplified and/or parametrised manoeuvres. The approach presented in this paper of using optimal control throughout, from reference generation to wheel torque allocation, represents a new approach to handling interventions at intersection accidents.

In future work, the robustness of the MHA, particularly with respect to the estimated friction level and tyre model inaccuracies will be analysed. The driver-interaction aspect of the function both in terms of response to the intervention and driver intention before the intersection needs to be studied. Lastly, full vehicle tests with the proposed controller for validation of the controller performance and demonstration of the real-time capability will be performed.

References

[1] NHTSA. Traffic Safety Facts 2009. Washington, DC: National Highway Traffic Safety Administra-

tion; 2009. Report No.: DOT HS 811 402; Available from: https://crashstats.nhtsa.dot.gov/Api/Public/ViewPublication/811402.

[2] Molinero Martinez A, Carter E, Naing C, Simon MC, Hermitte T. Accident causation and pre-accidental driving situations. Part 1 Overview and general statistics. 2008;:176.

[3] NHTSA. Fatality Analysis Reporting System (FARS) encyclopedia. 2017; Available from: https://www-fars.nhtsa.dot.gov/QueryTool/QuerySection/Report.aspx.

[4] European Commission. Traffic Safety Basic Facts on Junctions. European Commission, Directorate General for Transport; 2016. Report No.: bfs2016_junctions; Available from: https://ec.europa.eu/transport/road_safety/sites/roadsafety/files/pdf/statistics/dacota/bfs2016_junctions.pdf.

[5] Trafikanalys. Vägtrafikskador / Road traffic injuries. 2017 Apr; sveriges Officiella Statistik / Swedish Official Statistics; Available from: http://www.trafa.se/vagtrafik/vagtrafikskador/.

[6] Najm WG, Smith JD, Smith DL. Analysis of crossing path crashes. Cambridge, MA: NHTSA; 2001. Publication HS-809 423; Available from: https://trid.trb.org/view.aspx?id=718155.

[7] Najm WG, Ranganathan R, Srinivasan G, Smith JD, Toma S, Swanson E, Burgett A. Description of light-vehicle pre-crash scenarios for safety applications based on vehicle-to-vehicle communications. NHTSA; 2013. Publication DOT HS 811 731; Available from: https://trid.trb.org/view.aspx?id=1257636.

[8] Hafner MR, Cunningham D, Caminiti L, Vecchio DD. Cooperative Collision Avoidance at Intersections: Algorithms and Experiments. IEEE Transactions on Intelligent Transportation Systems. 2013 Sep;14(3):1162–1175.

[9] Misener JA. Cooperative intersection collision avoidance system (CICAS): Signalized left turn assist and traffic signal adaptation. University of California, Berkeley; 2010. Report No.: UCB-ITS-PRR-2010-20; Available from: https://trid.trb.org/view.aspx?id=919887.

[10] Pierowicz JA. Intersection collision avoidance using ITS countermeasures. ; 2000; Available from: http://hdl.handle.net/2027/mdp.39015075257181.

[11] Naumann R, Rasche R, Tacken J, Tahedi C. Validation and simulation of a decentralized intersection collision avoidance algorithm. In: Proceedings of Conference on Intelligent Transportation Systems; Nov.; 1997. p. 818–823.

[12] Naumann R, Rasche R. Intersection collision avoidance by means of decentralized security and communication management of autonomous vehicles. Univ.-GH, SFB 376; 1997; Available from: http://wwwcs.uni-paderborn.de/SFB376/projects/c1/Publications/Postscript/isata_in.ps.gz.

[13] Lytrivis P, Thomaidis G, Tsogas M, Amditis A. An Advanced Cooperative Path Prediction Algorithm for Safety Applications in Vehicular Networks. IEEE Transactions on Intelligent Transportation Systems. 2011 Sep;12(3):669–679.

[14] Boran C, Boström O, Jacobson B, Lie A, Sander U. Saving Lives with V2x versus On-Board Sensing Systems -Which will be More Effective? In: Chalmers Publication Library (CPL); 2012. Available from: http://publications.lib.chalmers.se/publication/185975-saving-lives-with-v2x-versus-on-board-sensing-systems-which-will-be-more-effective.

[15] Brännström M, Sandblom F, Hammarstrand L. A Probabilistic Framework for Decision-Making in Collision Avoidance Systems. IEEE Transactions on Intelligent Transportation Systems. 2013 Jun; 14(2):637–648.

[16] Brännström, Mattias. A Real-Time Implementation of an Intersection Collision Avoidance System. Aug.; 2011. p. 9794–9798; Available from: http://publications.lib.chalmers.se/publication/144752.

[17] Brännström M, Coelingh E, Sjöberg J. Model-Based Threat Assessment for Avoiding Arbitrary Vehicle Collisions. IEEE Transactions on Intelligent Transportation Systems. 2010;11(3):658–669.

[18] J Hillenbrand, AM Spieker, Kristian Kroschel. A Multilevel Collision Mitigation Approach -Its Situation Assessment, Decision Making, and Performance Tradeoffs. IEEE Transactions on Intelligent Transportation Systems. 2006 Dec;7(4):528–540.

[19] Lefèvre S, Bajcsy R, Laugier C. Probabilistic decision making for collision avoidance systems: Postponing decisions. In: 2013 IEEE/RSJ International Conference on Intelligent Robots and Systems; Nov.; 2013. p. 4370–4375.

[20] Eidehall A. Multi-target threat assessment for automotive applications. In: 2011 14th International IEEE Conference on Intelligent Transportation Systems (ITSC); Oct.; 2011. p. 433–438.

[21] Ammoun S, Nashashibi F. Real time trajectory prediction for collision risk estimation between vehicles. In: Intelligent Computer Communication and Processing, 2009. ICCP 2009. IEEE 5th International Conference on. IEEE; 2009. p. 417–422; Available from: http://ieeexplore.ieee.org/abstract/document/5284727/.

[22] Tamke A, Dang T, Breuel G. A flexible method for criticality assessment in driver assistance systems. In: 2011 IEEE Intelligent Vehicles Symposium (IV); Jun.; 2011. p. 697–702.
[23] Galvani M. Optimal-Control-Based Adas for Driver Warning and Autonomous Intervention Using Manoeuvre Jerks for Risk Assessment [dissertation]. University of Trento; 2013; Available from: http://eprints-phd.biblio.unitn.it/1131/.
[24] Gao Y. Model Predictive Control for Autonomous and Semiautonomous Vehicles. University of California, Berkeley; 2014; Available from: http://search.proquest.com/openview/fc42ec6b438e1446c5e7efc938360b20/1?pq-origsite=gscholar&cbl=18750&diss=y.
[25] Volvo Car Group (archive). City Safety with auto brake in intersections - Volvo Car Group Global Media Newsroom. 2017 Oct; Available from: https://web.archive.org/web/20171019063845/https://www.media.volvocars.com/global/en-gb/media/photos/148211/city-safety-with-auto-brake-in-intersections.
[26] Sander U. Opportunities and limitations for intersection collision interventionA study of real world left turn across path accidents. Accident Analysis & Prevention. 2017 Feb;99(Part A):342–355; Available from: http://www.sciencedirect.com/science/article/pii/S0001457516304493.
[27] Peter Janevik, Christian Berger, Magdalena Lindman, Per Gustafsson, Anna Wrige Berling, Mats Petersson. Final report, A-TEAM phase 1. Fordonsstrategisk forskning och innovation (FFI); 2015. Report No.: 2014-01397; Available from: http://www2.vinnova.se/PageFiles/751290059/2014-01397_EN.pdf.
[28] Bryson AE. Applied Optimal Control: Optimization, Estimation and Control. CRC Press; 1975; google-Books-ID: P4TKxn7qW5kC.
[29] Klomp M, Lidberg M, Gordon TJ. On optimal recovery from terminal understeer. Proceedings of the Institution of Mechanical Engineers, Part D: Journal of Automobile Engineering. 2014 Mar; 228(4):412–425; Available from: http://pid.sagepub.com/content/228/4/412.
[30] Gao Y, Lidberg M, Gordon T. Modified Hamiltonian Algorithm for Optimal Lane Change with Application to Collision Avoidance. MM Science Journal. 2015;(MAR 2015):576–584; Available from: http://www.mmscience.eu/content/file/MM%20SJ_201508.pdf.
[31] Gao Y, Gordon T, Lidberg M. Autonomous Emergency Cornering: Lane Departure Prevention for Highway Vehicles. In: Proceedings of the 2nd IAVSD Workshop on Dynamics of Road Vehicles. Berlin; 2017. Available from: http://www.iavsd-workshop2017.de/data/IAVSD_2017_Paper_Gao.pdf.
[32] Yang D, Gordon TJ, Jacobson B, Jonasson M. Quasi-Linear Optimal Path Controller Applied to Post Impact Vehicle Dynamics. IEEE Transactions on Intelligent Transportation Systems. 2012 Dec; 13(4):1586–1598.
[33] Gao Y, Gordon T, Lidberg M. Implementation of a modified Hamiltonian algorithm for control allocation. In: Advanced Vehicle Control: Proceedings of the 13th International Symposium on Advanced Vehicle Control (AVEC'16), September 13-16, 2016, Munich, Germany. CRC Press; 2016. p. 157; Available from: https://www.google.com/books?hl=en&lr=&id=8hINDgAAQBAJ&oi=fnd&pg=PA157&dq=yangyan+gao+tim+gordon&ots=ws4rQDWA6M&sig=0CK89tjj1YRdqIdzJTRo3wB8o0c.
[34] MSCSoftware. Adams Tire. In: Adams (2017.2) - Adams Docs. MSC.Software; 2017. DOC11449; Available from: https://simcompanion.mscsoftware.com/infocenter/index?page=content&id=DOC11449&cat=2017.2_ADAMS_DOCS&actp=LIST.
[35] Albinsson A, Bruzelius F, Gustafsson T, Jonasson M, Jacobson B. Identification of tyre characteristics using active force excitation. In: Chalmers Publication Library (CPL); 2015. Available from: http://publications.lib.chalmers.se/publication/221088-identification-of-tyre-characteristics-using-active-force-excitation.
[36] Albinsson A. Online State Estimation in Electrified Vehicles Linked to Vehicle Dynamics Licentiate thesis. Göteborg, Sweden: Chalmers University of Technology; 2015; Available from: http://publications.lib.chalmers.se/publication/223127-online-state-estimation-in-electrified-vehicles-linked-to-vehicle-dynamics.

Appendix A. Nomenclature

Symbol	Description
A	System state matrix
a_x, a_y	Longitudinal and lateral acceleration in vehicle frame
B	System input matrix

d	Global X-distance margin - distance between the host and the bullet vehicle at the end of the manoeuvre
F	Total force on particle in global reference frame
$\boldsymbol{f}$	System ode function
F_x, F_y, F_z	Longitudinal, lateral and vertical forces in vehicle frame respectively
F_{XG}, F_{YG}	Global X and Y forces respectively
$F^t_{x,i}, F^t_{y,i}$	Longitudinal and lateral force of tyre i in tyre reference frame
$F^v_{x,i}, F^v_{y,i}$	Longitudinal and lateral force of tyre i in vehicle reference frame
g	Acceleration due to gravity
H, H_i	Hamiltonian of vehicle and of tyre i
$H_{\beta,tol}, H_{\delta,tol}$	H_β and $H_{\dot{\delta}}$ tolerance thresholds around which the desired sideslip angle rate and desired steering rate switches smoothly from zero to k_β or $k_{\dot{\delta}}$ respectively - tunable parameters
$\mathbf{I}_{n\times n}$	n by n identity matrix
I_{zz}	Yaw moment of inertia
$J, J', \hat{J}$	Final, preliminary and augmented objective function
$k_\beta, k_{\dot{\delta}}$	Sideslip angle and steering rate constants - tunable parameters
m	Mass of the vehicle or particle
M_{ZG}, M_z, M^d_z	Global vehicle, estimated actual and desired yaw moment
O_X, O_Y	X and Y coordinates of the centre of the road segment arc
$\boldsymbol{p}$	Set of terminal constraints
$\mathbf{q}$	Input function for the particle model
R_{road}	Radius of the road segment arc
S	Maximum λ increment per iteration
t	Time
t_f	Duration of the manoeuvre
$\mathcal{U}$	Set of admissible control inputs
$\boldsymbol{u}$	Control inputs for the full vehicle model
v_b	Bullet vehicle velocity
v_x, v_y	Longitudinal and lateral velocities in vehicle frame
v_0	Host vehicle initial velocity
X, Y	Global X and Y positions respectively
$\boldsymbol{x}$	System state vector
X_{b0}	Global X-distance between the host and the bullet vehicle at the beginning of the manoeuvre
x_i, y_i	x and y distance of wheel i from the centre of gravity in vehicle reference frame
α_i	Slip angle of tyre i
β	Vehicle sideslip angle
β_1, β_2	Lower and upper sideslip angle thresholds for sideslip control
$\dot{\beta}^d$	Desired sideslip angle rate
$\boldsymbol{\gamma}$	Control inputs for the particle model
$\delta, \delta_i, \delta_{whl}$	Steering wheel angle, steering angle of wheel i and average steer angle at front wheels
$\dot{\delta}^d$	Desired steering angle rate
ϵ	Yaw moment difference scaling factor
$\boldsymbol{\eta}$	Lagrange multipliers for terminal constraints
θ_0, θ_f	Initial and final angle subtended by the host vehicle position and the centre of the road segment arc to the vertical

$\boldsymbol{\lambda}$	Lagrange multipliers for the system equations
λ	Lagrange multiplier for yaw moment in the MHA
μ	Road friction coefficient
ν, ν^d	Actual and desired course angle
τ	Desired yaw response time constant
ϕ, ϕ_v	Force angle in global and vehicle reference frame
$\phi_{t,i}, \phi_{w,i}$	Force angle of tyre i in tyre reference frame and of wheel corner i in vehicle reference frame
ψ	Yaw angle
ω_z, ω_z^d	Actual and desired yaw rate
$\mathbf{0}_{n\times n}$	n by n null matrix